Accepted Manuscript

Finite element prediction of resin pocket geometry around embedded optical fiber sensors in prepreg composites

Nicolas Lammens, Geert Luyckx, Eli Voet, Wim Van Paepegem, Joris Degrieck

Finite element prediction of resin pocket geometry around embedded optical fiber sensors in prepreg composites

Nicolas Lammens[1*], Geert Luyckx[1], Eli Voet[1], Wim Van Paepegem[1], Joris Degrieck[1]

[1] Department of Materials Science & Engineering, UGent
Technologiepark-Zwijnaarde 903
B-9052 Zwijnaarde
Belgium
* Corresponding author: Nicolas.Lammens@ugent.be

Abstract

This work presents a finite element technique allowing for the accurate prediction of resin pocket geometries surrounding optical fiber sensors in UD prepreg composites. The F.E. implementation solely relies on material models and element formulations readily available in all commercial F.E. codes, rather than requiring specialized user developed element and material formulations. In addition, only a minimal amount of straight-forward experimental characterization is required to determine the necessary material parameters in the model. The F.E. results are validated with microscopic images of several lay-ups with embedded optical fiber samples of different diameters. Very good correspondence is found between F.E. results and microscopic cross-sections, showing the usefulness and applicability of the method to random lay-ups and optical fiber dimensions.

Keywords: optical fiber, composites, finite element

Introduction

With the increasing use of composite materials, much research is being performed into the concept of 'smart structures'. Equipped with a multitude of sensors, these structures are capable of responding to certain inputs ranging from the more basic stress/strain sensing, to more advanced features such as morphing geometries and structural health monitoring. The EU FP7 'SmartFiber' project (2010 – 2014) even aims at embedding both sensor and read-out equipment inside the composite host, providing a fully embedded health-monitoring system. By embedding the sensor and read-out system during production of the part, these parts are protected from environmental factors while at the same time providing the additional capability of monitoring the production cycle. However, due to the fibrous nature of composite structures, the presence of any foreign structure will distort the surrounding material and impact the performance of the final part [1-9]. These distortions will impact both the accuracy of the sensor as well as the fatigue behavior of the structure, and must therefore be analyzed and reduced if possible.

When optical fiber sensors are embedded off-axis (relative to the reinforcements) in laminated composites, a characteristic lenticular 'resin pocket' occurs around the optical fiber sensor. Shivakumar et al. [8] investigated the resin-rich zones surrounding a polyimide coated optical fiber, embedded in a unidirectional carbon/epoxy laminate. It was observed that the resin-rich zones

surrounding the optical fiber sensor significantly affect the compression strength of the host material. Strength reductions up to −40% were reported for samples in which the optical fiber was oriented perpendicular to the reinforcements. The tensile modulus and strength were found to be reduced by approximately −5% for this optical fiber orientation. Surgeon et al. [9] published similar experimental data on static and dynamic testing of quasi-isotropic carbon fiber epoxy laminates with embedded optical fibers. It was shown that under tensile loading, only small influences of the optical fiber on tensile stiffness and strength could be detected, while the influence was much more pronounced for bending experiments. The samples in which the optical fiber was embedded between a 0 ° and 45 ° layer, with the optical fiber oriented in the 90 ° direction showed the largest degradation, up to 51%. Lee et al. [4] performed experimental tests to determine the influence of embedded fiber optics in both static and fatigue samples using glass-epoxy prepregs. An acrylate coated fiber was used in all samples. Under static load conditions, the presence of an optical fiber had no significant influence on tensile stiffness or strength. In fatigue loading however, a significant decrease in fatigue lifetime was found when optical fibers were present. Herranen [10] performed research into smart structures in which electronics are embedded inside the composite host for sensing purposes. To study the effects of inclusion geometry on the resulting resin pockets and structural performance of the host, an extensive experimental program was developed testing several laser sintered PA12 geometries as inclusions. It was found that the precise inclusion geometry had a measurable influence on structural strength, and an optimal geometry could be determined to minimize the effect of the inclusion.

The reductions in stiffness and strength reported in the research described above, can be attributed to the local distortion of the laminate surrounding the optical fiber, and the creation of resin-rich zones. As these resin pockets have a significant effect on the structural behavior of the part, a tool capable of predicting these resin pocket geometries and consequently the influence on mechanical behavior is necessary to ensure the reliability and safety of these structures.

Dasgupta et al. [11] presented an analytical framework to determine the resin pocket geometry based on easily accessible material properties such as reinforcing fiber stiffness and diameter. Dasgupta approximated the resin pocket geometry by a series of beam functions. While good correspondence with microscopic images was achieved, personal correspondence with Dasgupta revealed that the convergence of the algorithm proved very difficult and time consuming. Case et al. [12] modified the energy formulation presented by Dasgupta and used a sinusoidal displacement field rather than a series of beam functions. The resulting simplifications allowed the author to extract an analytical expression for the resin pocket geometry. Her et al. [13] considered that the resin pocket is not necessarily symmetric through the thickness of the laminate, and modified the formulation given by Dasgupta to account for this effect.

Even though the work published by Dasgupta, Case and Her show good correspondence with experimental results, they are only applicable for optical fibers which can be regarded as infinitely long and straight. Hence, these approaches are no longer valid in situations where curved optical fiber paths are

envisaged, or when other types of embedded structures (with more complex geometries than simple circular extrusion profiles) are considered. The use of finite element techniques, as presented in this work, overcomes this fundamental issue and can potentially predict resin pockets surrounding any kind of inclusion geometry. Additionally both Case and Her calculate the bending energy of the laminate as $U_b = \frac{1}{2}\int_V E_x \left(\frac{\partial^2 v}{\partial x^2}\right)^2 y^2 dV$ with variable stiffness to account for different orientations of plies. This effectively means that the entire laminate is regarded as one solid part under bending deformations. However, it is well known that the bending stiffness of uncured laminates is much lower because of sliding between the reinforcing layers.

This work will present an alternative method to the determination of resin pocket geometry, based on F.E. formulations. Although a lot of research has been performed into the macro-scale drape behavior of composites [14-16], these methods often use proprietary codes and material models, which require extensive material characterization and validation of the coding. The approach proposed in this work differs from these drape simulations by relying solely on standard elements, material models and F.E. formulations. It is recognized that this objective will entail some sacrifices in the modeling accuracy of the complex forming phenomena involved. However, the principal purpose of these efforts is to obtain an easy-to-use, straight-forward tool that will allow the quick determination of cured part geometry of composites with embedded sensors, rather than have an accurate model of the precise forming behavior. Additionally, for the simulation of UD materials, the required material characterization is limited to very basic tests. Compared to the analytical method proposed by Dasgupta, the proposed model is more flexible as it allows the user to simulate any form of inclusion.

In the next section, an overview of the experimental samples created for the purpose of validating F.E. prediction is given, as these will also be used as a way to visually extract some material properties. Next, an overview of the dominant deformation modes in composite forming is given, and the modelling objectives of this work are discussed. The different deformation modes are used as a starting point to determine the necessary material parameters. The method is applied to the specific case of a carbon fiber unidirectional (UD) prepreg (Hexcel M18/M55J) used for illustration purposes through-out this work. Finally, the obtained material properties are used in a finite element simulation and compared to microscopic images of the experimental samples created.

Embedded optical fiber samples

As the resin pocket geometry is strongly dependent on the relative orientation of the optical fiber with regard to the surrounding reinforcements, several samples were created in order to validate the accuracy of the finite element implementation. All samples were made using M18/M55J UD carbon fiber epoxy prepreg manufactured by Hexcel and cured in an autoclave cycle according to the manufacturer specifications. The samples were manufactured using the vacuum-bagging technique without using a caul-plate on the top surface. All samples contain Ormocer$^{\circledR}$ coated optical fiber sensors of different diameter, produced using a draw-tower fiber process manufactured by FBGS Technologies. The different sample lay-ups, diameter of optical fiber and number of cross-

sections are given in Table 1. The lay-up angles are given relative to the optical fiber orientation (oriented in the 0 ° direction).

Table 1 Details of sample lay-up

Specimen name	Stacking sequence	Number of cross sections
UD-90-1	90_2/**OF-125**/90_2	3
UD-90-2	90_4/**OF-125**/90_4	3
UD-90-3	90_{16}/**OF-125**/90_{16}	3
UD-45-1	45_2/**OF-60**/45_2	3
UD-45-2	45_2/**OF-80**/45_2	1
UD-45-3	45_2/**OF-125**/45_2	3
CP-1	0_2/90_2/0_2/90_2/**OF-60**/90_2/0_2/90_2/0_2	3
CP-2	0_2/90_2/0_2/90_2/**OF-80**/90_2/0_2/90_2/0_2	3
CP-3	0_2/90_2/0_2/90_2/**OF-125**/90_2/0_2/90_2/0_2	3

OF-60: 60μm fiber, 106μm coating
OF-80: 80μm fiber, 129μm coating
OF-125: 125μm fiber, 200μm coating

After curing, all samples are cut perpendicular to the optical fiber, polished and examined under an optical microscope with calibrated magnifications, allowing the measurement of distances on the recorded images. Figure 1 shows the resulting cross-sections for samples of type UD-90-1, UD-45-1 and CP-3. Several cross-sections were created across the length of the cured samples, showing only small variations in the resin pocket geometry.
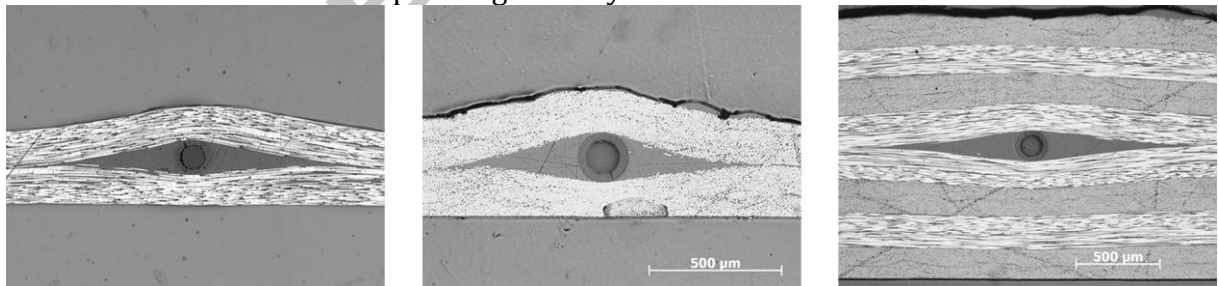

Figure 1 Microscopic images of carbon fiber reinforced laminates with embedded optical fibers (l-t-r: UD-90-1, UD-45-3, CP-3)

The microscopic cross-sections are purely intended to serve as validation of the developed material model. By considering different lay-ups, laminate thicknesses and inclusion sizes, the validity of the (single) material model developed in this work is evaluated over a wide range of circumstances. The material parameters determined in the following section are purely based on data obtained from a separate bending test, theoretical considerations and datasheets from manufacturers, and do not rely on these microscopic images. The microscopic samples described here are only used at the final stage of validation, and to allow final fine-tuning of those material properties which could not be determined precisely.

Modelling approach

Many different approaches can be found in literature on how to model the curing of a reinforced epoxy. A very common approach leading to accurate cure simulations is to use a so-called 'cure hardening instantaneously linear elastic' (CHILE) model in which the assumption is made that at every point in time the laminate responds in a linear elastic way, but with an elasticity which evolves through time. It has been shown that a properly calibrated CHILE model produces equivalent results as visco-elastic modeling, at only a fraction of the computational cost [17]. Considering that the forming of the resin pocket will take place in the early stages of the curing process (when viscosity is low), the CHILE model can be reduced to a purely elastic material model. In this work, the methodology presented will be applied to a UD carbon-fiber prepreg (Hexcel M18/M55J). As the used M18/M55J prepreg is unidirectional, the material model should exhibit transverse isotropic behavior. Consequently, a linear elastic transverse isotropic material model will be used. While the model is equally applicable to fabrics, the loss of transverse isotropy in these materials will necessitate some additional tests and/or assumptions to derive all required material properties.

In the past, researchers have shown that composite forming is dominated by (i) intra-ply shearing, (ii) intra-ply tensile loading, (iii) ply/ply and ply/tool shearing, (iv) ply bending and (v) compaction/consolidation [18]. These deformation modes will be used to determine or estimate the necessary material parameters for the material model used in our analysis.

<u>Decoupling bending and in-plane behavior</u>

In composite forming, the in-plane properties (i.e. intra-ply shearing and tensile loading) are decoupled from the bending response of a single ply. On the contrary, finite element implementations assume that bending stiffness is derived from in-plane material response. In order to decouple the in-plane behavior of the ply from the bending behavior, a single ply will be modeled as a stack of individual layers held together by friction. This is illustrated in Figure 2 (left) for the simplified case of a single ply being represented by three individual layers. In the next sections, the necessary material parameters for the individual layers as well as the required amount of layers per ply will be determined based on data available from experimental tests and/or datasheets and literature data.
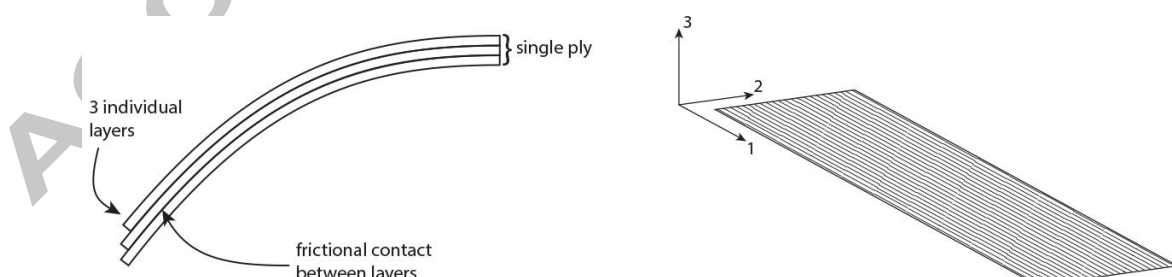

Figure 2 (left) Layered ply modeling approach, (right) default coordinate system

A default coordinate system is used as shown in Figure 2 (right).In this default coordinate system, the 1-direction corresponds to the reinforcement direction. The 2 direction is perpendicular to the reinforcements within the plane of the ply, while the 3 direction is in the through-thickness direction of the ply. This

coordinate system will be used in the determination of the material properties described next.

Intra-ply shearing

Intra-ply shearing in (dry) fabric materials is usually dominated by shear effects between the warp and weft directions of the fabric. The determination of the intra-ply shear in these materials is obtained by either a picture frame test or a bias extension test. In a prepreg UD material however, this interaction between warp and weft disappears and only the matrix material is responsible for shear effects. While picture frame tests could be used to determine the shear response of these materials, an extensive amount of tests would be necessary in order to obtain the shear behavior as a function of time and temperature. In order to avoid these extensive tests, the intra-ply shear behavior is determined using an iterative F.E. process until correspondence with experimental results is obtained. Based on theoretical considerations, the range of allowable shear moduli is restricted:

- Because of the transverse isotropy of the UD plies, $G_{12}=G_{13}$ (with the 1-direction parallel to the reinforcement direction)
- Assuming the 1-direction to always represent the stiffest direction in the ply, while the 2-direction (and equivalently the 3-direction) represents the weakest direction further restricts the range of allowable shear moduli: $20MPa < G_{12} < 100GPa$. These limits are determined by requiring that no coordinate transformation of the stiffness matrix should result in either a stiffer or weaker direction than the 1- or 2-direction respectively.
- Finally, the uncured shear modulus should be lower than the cured shear modulus ($G_{12} = 4300MPa$). Consequently, $20MPa < G_{12} < 4300MPa$.

Several values of G_{12} within this range of allowable values were considered. It was found that changing the value of G_{12} had only minute influences on the final resin pocket geometry. This can be explained by the fact that most of the actual shear deformation is transformed into frictional sliding by the layered build-up of a single ply. As the value of G_{12} is decreased, the anisotropy of the material becomes more and more pronounced leading to stability issues in the numerical algorithm. It was found that values below $G_{12} = 300$ MPa resulted in very small time-increments (and corresponding high calculation times), while the changes in resin pocket geometry were nearly indistinguishable. Taking into account that the choice of G_{12} value over the entire allowable range had only minimal effects on resin pocket geometry, and that intuitively low shear stiffness values are expected, the lowest stable value of $G_{12} = 300$ MPa was selected for this material. Note that, in order to account for the low bending stiffness of the ply, a single ply is modeled as a number of individual layers held together by friction (Figure 2(left)). The determined shear modulus $G_{12} = 300MPa$ represents the shear stiffness of a single (fictitious) layer, and should not be compared to shear moduli published in literature (<1MPa for Toray T800SC/3900-2B carbon-fiber uncured, heated thermoset epoxy [19]). Under most load conditions, the (finite element) shear behavior on a ply level is expected to be dominated by friction between the individual layers rather than shearing within the individual layers, and thus represent a very low (effective) shear stiffness for the entire ply.

Intra-ply tensile loading

Assuming that when the resin pocket is formed, the low-viscosity uncured epoxy has a negligible load-bearing capacity, the intra-ply tensile loading behavior in

the reinforcement direction is determined solely by the reinforcement fibers and the fiber volume fraction. The uncured (as-delivered) volume fraction of carbon fibers in the Hexcel M18/M55J prepreg used for this analysis is stated to be 55.21% by the manufacturer. According to the datasheet for the Toray M55J carbon fiber, the axial tensile modulus of M55J is 540 GPa. Consequently, the uncured stiffness along the reinforcement direction is determined to be E_{11} = 298 GPa.

Ply/ply shearing

Generally, ply/ply shearing is found to be both pressure and rate dependent. However, the tests to determine these dependencies require specialized equipment beyond the aims of this work. Consequently, a constant coefficient of friction will be assumed to model the ply/ply shearing behavior. Note that this does not affect the general usability of the presented approach, as most F.E. software codes allow for pressure-dependent contact formulations if desired. For the analysis of the M18/M55J carbon fiber prepreg, a coefficient of friction μ = 0.14 is used corresponding to a general value for lubricated carbon-carbon friction. This value is within the range of experimental measurements on comparable HexPly T700/M21 (μ=0.22) and HexPly AS4/8552 (μ=0.12) carbon-fiber prepregs from Hexcel [20].

Ply bending

As a result of sliding between the separate reinforcement fibers in a single composite ply, the bending stiffness of these materials is significantly lower than what would be derived from the in-plane material properties using beam or plate theory. In order to obtain proper drape simulations however, it is necessary that both the in-plane and bending behavior are modeled correctly. This poses a significant issue as none of the standard material models and element types implemented in ABAQUS allow the decoupling of tensile stiffness and bending stiffness.

In most drape modeling research, the bending stiffness is either completely ignored by using membrane elements (i.e. shell elements with no bending stiffness), or specialized user elements are written which decouple bending and in-plane behavior. While ignoring bending stiffness is acceptable in certain large scale experiments, it cannot be ignored in the forming of resin pockets. Additionally, using membrane elements would prohibit modeling of through-thickness compaction which is discussed next. Custom-coded user elements on the other hand, are considered outside the scope of this work. Although these user elements have their merits and benefits, the required expertise in computational mechanics in order to develop a (physically meaningful) user element, will restrict the use of the method to a small sub-set of researchers with the proper background. In addition, these user elements generally require extensive testing and validation, combined with advanced material characterization before accurate simulations are viable. As the objective of this work is to develop an easy-to-use, straightforward modelling approach accessible to a wide array of researchers (including those focusing on the experimental application of optical fiber sensors or structural health monitoring in general, rather than having a profound understanding of finite element methods), user elements will not be considered in this work. Readers interested in user-elements are referred to relevant literature on the matter [14-16].

In the F.E. implementation used in this work, the bending behavior is decoupled

from the in-plane properties by separating a single ply into several individual layers held together by friction (Figure 2(left)). The in-plane properties of the individual layers correspond to the in-plane behavior of the ply, while the amount of layers is varied to obtain the proper bending behavior.

In order to estimate the bending stiffness of the prepreg material used, without the need for expensive test equipment, a simple cantilever test was performed in which a single ply is heated (to 180°C, the curing temperature specified for this material) and allowed to bend under the influence of gravity. The resulting cured geometries for different lengths of material are shown in Figure 3.

Figure 3 Cured geometry of cantileverd M18/M55J prepreg samples

Different lengths of prepreg were tested. The width of all samples was kept to a minimum (10mm) in order to avoid plate effects. After curing, the vertical displacement was measured. The determined displacements are gathered in Table 2. Note that because of the large displacements, standard beam theory is no longer valid for these experiments. Modified formulations need to be used in order to determine the bending stiffness from these results [21].

Table 2 Vertical displacements for various sample lengths under cantilever loading during curing

Sample length	Vertical displacement
50mm	7mm
70mm	21mm
90mm	45mm
110mm	76mm
130mm	120mm
150mm	140mm

Using the differential equation approach to the Peirce cantilever test presented in [21] it is possible to simulate the bending behavior of a composite ply for different values of bending stiffness. Using a least-squares fit between the theoretical and experimental displacements (Table 2), the bending stiffness of the ply is determined. A mass density =1.62g/cm^3 is used, as stated by the manufacturer. Figure 4 shows the theoretical and experimental displacements resulting in the lowest difference between theory and experiment.
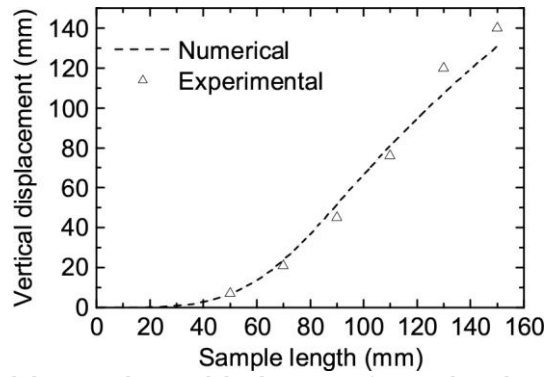
Figure 4 Experimental and theoretical vertical displacements for cantilever bending of uncured M18/M55J prepreg

Using this technique, the bending stiffness of a single M18/M55J prepreg ply is determined to be 0.2026Nmm². Given an uncured ply thickness of 105μm, this is then found to be equivalent to either 11 stacked layers with E_{11} = 254GPa or 12 layers with E_{11} = 302GPa to obtain the desired bending behavior (in absence of friction). As friction between the individual layers of the ply will result in a slight increase of the ply bending stiffness, the bending behavior is modeled using 12 layers per ply with E_{11} = 298GPa.

Compaction/consolidation

During curing of a composite, significant compaction of the fiber bed occurs due to the application of pressure. Additionally, during the curing process, epoxy is extracted from the prepreg into the breather/bleeder material under the influence of external pressure, leading to a globally thinner cured part and higher volume fraction. A simple relationship between volume fraction V_f and curing pressure (P) has been proposed based on experimental results [18]:

$$V_f = V_0 P^B \tag{1}$$

in which B is an empirical factor called the stiffening index, V_0 the initial (as-delivered) volume fraction and V_f the final volume fraction. Correia [22] investigated the relationship between V_0 and B and proposed a logarithmic equation based on least-square fitting of experimental data from vacuum infused parts:

$$B = -0.06567 \ln V_0 - 0.02745 \tag{2}$$

Based on measured cured-ply-thickness (CPT) values of the UD-90 samples, an average CPT of 95μm was found. This equates to a cured fiber volume fraction of 61.06% according to the manufacturer. A total pressure of 8 bar (7 bar nitrogen + 1 bar vacuum) was used in the curing of the samples. From Equation (1), a stiffening index B =0.0151 is obtained, while the logarithmic fit (Equation (2)) results in a predicted B =0.0116. Considering that Equation (2) was derived mainly for low V_0 values and in vacuum infused parts (i.e. without using bleeder/breather material), this correspondence is rather good.

Using the measured ply thickness and applied pressure, a linear through-thickness stiffness of $E_{22} = E_{33}$ =8.4MPa is obtained. However, considering that $t \sim \dfrac{1}{V_f}$ with t representing the cured ply thickness, Equation (1) shows that ply compaction cannot be captured accurately using a purely linear assumption. While the overall simulated resin pocket geometry was very good using E_{22} = 8.4 MPa, simulations showed that this value led to a slight over-estimation of laminate compression underneath the optical fiber sensor, when compared to

the microscopic samples. Although the extent of this over-estimation is limited to narrow region directly underneath the optical fiber (where a stress concentration occurs during forming), an increase in transverse stiffness to E_{22} = E_{33} = 13.5MPa was found to achieve better correspondence. In order for the global response of the ply to remain correct (i.e. compress to 95µm under 8 bar of pressure), the initial thickness of the ply has to be reduced to 101µm. Finally, a distinction must be made between plies above the optical fiber and those below. As a first assumption, the bottom layers must behave according to the compaction behavior described previously. However, the top layers will respond differently since in reality epoxy in these layers can flow out towards the breather/bleeder material or into the resin pocket. This flowing behavior cannot be modeled by the simplified linear elastic F.E. implementation and would result in incorrect deformations of the top plies. In order to resolve this issue, the top layers are modeled as if all excess epoxy was already removed prior to the simulation. As a result, the top layers have a layer thickness equal to the CPT (95µm) and no further compression of these plies is needed. Therefore an increased transverse stiffness is necessary for these layers. Although any value of E_{22} sufficiently higher than 13.5 MPa can be chosen – in order to ensure compression of the plies happens in the bottom layers and not in the top layers –, an arbitrary value of 40 MPa was selected. This was found to be sufficient to concentrate (most of) the compression to the bottom plies and obtain a computationally stable material model (i.e. large differences in E_{22} between top and bottom layers may lead to difficult convergence of the F.E. algorithm).

Poisson coefficient

During the first stages of curing, the epoxy can be thought of as being a liquid and therefore incompressible. Using the orthotropic material properties derived previously, incompressibility would require $v_{12} = v_{13} = 0.5$ and $v_{23} = 0.99$. However, this does not account for the ability of the resin to fill the resin pocket or being extracted into the breather/bleeder material. Therefore (especially for plane strain simulations as performed in this work where flow out of the modelling plane is prohibited), the strict incompressibility needs to be reduced in the transverse 2-3-plane. For simplicity $v_{12} = v_{13} = v_{23} = 0.5$ is chosen. This was found to significantly improve the convergence of the F.E. algorithm, and produce identical results to a 3D simulation (using an incompressible material definition) allowing the resin to "flow" in the extrusion direction of the optical fiber.

All relevant (uncured) material parameters are collected in Table 3. The parameters marked with an asterisk (*) are parameters which were modified after comparison with microscopic cross-sections, rather than based on datasheets or experimental tests. For these parameters, it was found that the precise value had only a minimal influence on the predicted resin pocket geometry, but either improved the general performance of the simulation or resulted in a slightly improved (localized) correlation to the microscopic samples. It is important to note that these are fine-tuning efforts, and using the default values as derived in the previous sections will still lead to a very good correspondence to experimental results!

Table 3 Uncured M18/M55J prepreg material properties

	Top layers	Bottom Layers	
Layers per ply	12	12	
Ply thickness	95μm	101μm	
ρ	1.62 g/cm³	1.62 g/cm³	
E_{11}	298 GPa	298 GPa	
$E_{22} = E_{33}$	40 MPa	13.5 MPa	*
$\nu_{12} = \nu_{13} = \nu_{23}$	0.5	0.5	*
$G_{12} = G_{13}$	300 MPa	300 MPa	*
G_{23}	13 MPa	13 MPa	

Finite element model

Using the material properties as defined in Table 3, the drape behavior is modeled using a 2D generalized plane strain approach. Each ply is modeled using 12 individual layers with 7140 CPEG4 elements per ply. A mesh-convergence study was performed, showing that this number of elements was sufficient to accurately capture the resin pocket geometry. Contact is defined between all surfaces using μ = 0.14. The individual surfaces are not allowed to separate after they have made contact. The contact between the laminate and optical fiber was modeled as being frictionless. The model is subjected to a combination of gravity loading and pressure loading (8 bar) applied to the top surface of the laminate. The F.E. model, boundary conditions and loads are shown in Figure 5 for a [90_2,OF-125,90_2] lay-up. For clarity, the mesh is not shown in this figure.
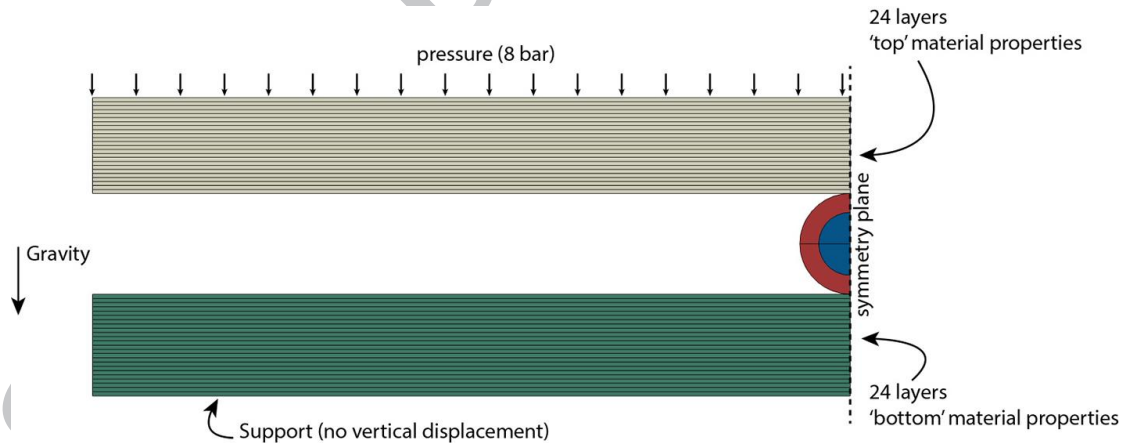

Figure 5 F.E. model and boundary conditions

Optical fiber properties

The optical fiber is modeled as an isotropic material with E = 72.4GPa and $\nu = 0.16$. While temperature dependency of the elastic modulus and Poisson's ratio of silica has been reported in literature (E = 72.2+0.0096·T GPa [23]) these small variations are assumed to be negligible in the final resin pocket geometry. However, Voet [24] showed that the Ormocer® coating material properties are strongly dependent on temperature. Using the experimental data given in [24], the Ormocer® elastic modulus is extrapolated at the cure temperature of 180°C, and found to be E = 200 MPa. The Poisson coefficient is assumed to remain unaffected at $\nu = 0.32$.

Results

Figure 6 shows the predicted finite element resin pocket geometries superimposed on top of the microscopic cross-sections. The F.E. curves were scaled based on the magnification scales of the microscopic images in order to enable a direct comparison between experiment and F.E. results.
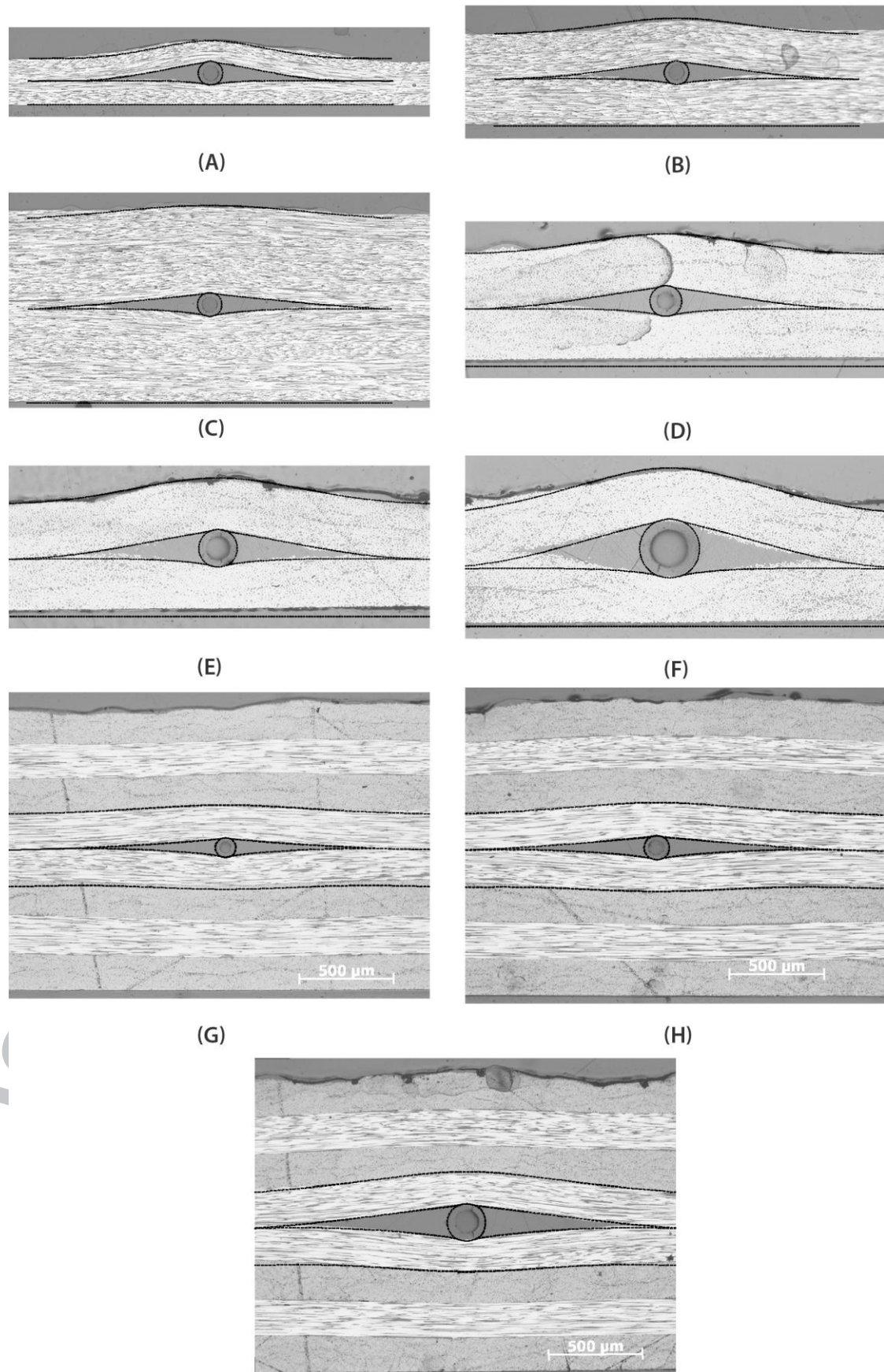
Figure 6 Resin pocket and F.E. predictions (dotted lines): (a) UD-90-1, (b) UD-90-2, (c) UD-90-3, (d) UD-45-1, (e) UD-45-2, (f) UD-45-3, (g) CP-1, (h) CP-2, (i) CP-3

The results shown in Figure 6 show an almost perfect correspondence to the actual resin pocket geometry. It is also shown that the resin pocket geometry differs greatly depending on factors such as ply count (6(a) – (c)), inclusion size (6(d) – (f)), and stacking sequence (6(c), 6(f) and 6(i)).

It should be reminded that the determination of the F.E. material model did not rely on comparison or parameter tuning to these microscopic images, but was based purely on separate bending tests, theoretical considerations and datasheet information. Only the E_{22} value was modified slightly based on the UD-90-1 image, as it was discussed that a linear approach would not be able to accurately model the compression response. In addition, the modifications to E_{22} only influence a narrow region below the optical fiber, and do not affect the overall resin pocket geometry.

The correspondence between F.E. simulations and experimental results is very good, and is expected to be sufficiently accurate for most applications requiring knowledge of the resin pocket geometry. The model accurately captures the resin pocket geometry in all cases considered. Considering that these results were achieved using a very limited amount of input (datasheets, bending test) and a standard transversely isotropic material model, the results clearly illustrate the significant benefits of the method compared to the analytical methods proposed which lack flexibility and require extensive programming. In addition, the method only takes minutes to converge, with convergence times mainly attributed to element count rather than numerical difficulties.

Conclusion

In this work, a finite element approach was demonstrated in order to accurately predict the resin pocket geometries surrounding optical fiber embedded in prepreg composites. The modeling approach and determination of necessary (uncured) material properties was discussed in detail, including a technique for determining bending stiffness of high-temperature curing prepregs. Only a straightforward bending tests and manufacturer datasheets were required to derive all necessary material parameters. The accuracy of the method was validated by comparison to microscopic images. The implementation of the F.E. approach was shown to yield very good correspondence for all microscopic images considered, including variations in laminate thickness, layer stacking and inclusion dimensions. Compared to the approaches available in literature, the F.E. implementation is more flexible as it requires no assumptions on allowable displacement functions.

Acknowledgement

References

[1] Benchekchou B, Ferguson NS. The effect of embedded optical fibres on the fatigue behaviour of composite plates. Compos Struct. 1998;41(2):113-20.

[2] Choi C, Seo DC, Lee JJ, Kim JK. Effect of embedded optical fibers on the interlaminar fracture toughness of composite laminates. Compos Interface. 1998;5(3):225-40.

[3] Hadzic R, John S, Herszberg I. Structural integrity analysis of embedded optical fibres in composite structures. Compos Struct. 1999;47(1-4):759-65.

[4] Lee DC, Lee JJ, Yun SJ. The Mechanical Characteristics of Smart Composite Structures with Embedded Optical-Fiber Sensors. Compos Struct. 1995;32(1-4):39-50.

[5] Ling HY, Lau KT, Lam CK. Effects of embedded optical fibre on mode II fracture behaviours of woven composite laminates. Compos Part B-Eng. 2005;36(6-7):534-43.

[6] Melin LG, Levin K, Nilsson S, Palmer SJP, Rae P. A study of the displacement field around embedded fibre optic sensors. Compos Part a-Appl S. 1999;30(11):1267-75.

[7] Seo DC, Lee JJ. Effect of Embedded Optical-Fiber Sensors on Transverse Crack Spacing of Smart Composite Structures. Compos Struct. 1995;32(1-4):51-8.

[8] Shivakumar K, Emmanwori L. Mechanics of failure of composite laminates with an embedded fiber optic sensor. J Compos Mater. 2004;38(8):669-80.

[9] Surgeon M, Wevers M. Static and dynamic testing of a quasi-isotropic composite with embedded optical fibres. Compos Part a-Appl S. 1999;30(3):317-24.

[10] Herranen H. Design Optimization of Smart Composite Structures with Embedded Devices: Tallinn University of Technology; 2014.

[11] Dasgupta A, Wan Y, Sirkis JS. Prediction of resin pocket geometry for stress analysis of optical fibers embedded in laminated composites. Smart Materials and Structures. 1992;1(2):101.

[12] Case SW, Carman GP. Compression Strength of Composites Containing Embedded Sensors or Actuators. J Intel Mat Syst Str. 1994;5(1):4-11.

[13] Her SC, Yao BR, Lan SC, Liu CY. Stress Analysis of a Resin Pocket Embedded in Laminated Composites for an Optical Fiber Sensor. Key Eng Mat. 2010;419-420:293-6.

[14] Badel P, Gauthier S, Vidal-Salle E, Boisse P. Rate constitutive equations for computational analyses of textile composite reinforcement mechanical behaviour during forming. Compos Part a-Appl S. 2009;40(8):997-1007.

[15] Hamila N, Boisse P. A meso-macro three node finite element for draping of textile composite preforms. Appl Compos Mater. 2007;14(4):235-50.

[16] Hamila N, Boisse P, Sabourin F, Brunet M. A semi-discrete shell finite element for textile composite reinforcement forming simulation. Int J Numer Meth Eng. 2009;79(12):1443-66.

[17] Zobeiry NRAVRPA. Efficient Modelling Techniques for Predicting Processing Residual Stress and Deformation in Composite Parts. ICCM14. San Diego, California, USA2003.

[18] Long AC. Composites Forming Technologies: Elsevier Science; 2007.

[19] Kofoid J. Constitutive Modeling of Advanced Thermoset Composites with Application to Sheet Forming Processes [PhD]. Berkeley: University of California; 2001.

[20] Larberg YR, Akermo M. On the interply friction of different generations of carbon/epoxy prepreg systems. Compos Part a-Appl S. 2011;42(9):1067-74.

[21] Lammens N, Kersemans M, Luyckx G, Van Paepegem W, Degrieck J. Improved accuracy in the determination of flexural rigidity of textile fabrics by the Peirce cantilever test (ASTM D1388). Text Res J. 2014.

[22] Correia NACM. Analysis of the vacuum infusion moulding process [PhD]. Nottingham: University of Nottingham; 2004.

[23] Fukuhara M, Sanpei A, Shibuki K. Low temperature-elastic moduli, Debye temperature and internal dilational and shear frictions of fused quartz. J Mater Sci. 1997;32(5):1207-11.

[24] Voet E. In-situ deformation monitoring of aerospace qualified composites with embedded improved draw tower fibre Bragg gratings. Ghent, Belgium: Ghent University. Faculty of Engineering and Architecture; 2011.